PCCP

PAPER

View Article Online
View Journal | View Issue

Cite this: *Phys. Chem. Chem. Phys.*, 2025, **27**, 23428

Strong-field induced ionization and dissociation of *cis*- and *trans*-1,2-dichloroethylene: Cl^+ and HCl^+ fragments

Ephraim Anto,[a] Rituparna Das,[b] Vinitha Nimma,[b] Madhusudhan P,†[b] Pranav Bhardwaj,‡[b] Pooja Chandravanshi,[b] Rajesh Kumar Kushawaha[b] and Koushik Saha*[a]

Received 8th August 2025,
Accepted 29th September 2025

DOI: 10.1039/d5cp03038b

rsc.li/pccp

Strong-field induced ionization of polyatomic molecules using femtosecond laser pulses leads to complex fragmentation dynamics like bond-breaking, intramolecular proton migration, roaming, bond formation, and Coulomb explosion. In this work, we report the strong-field induced ionization and dissociation dynamics of *cis*- and *trans*-1,2-dichloroethylene (DCE) employing ion momentum spectroscopy with multi-ion coincidence detection of fragment ions. Two-body dissociation from the doubly ionized molecular ion involving Cl^+ ejection, *i.e.*, the $Cl^+ + C_2H_2Cl^+$ channel, and HCl^+ ejection, *i.e.*, the $HCl^+ + C_2HCl^+$ channel, is studied in detail as a function of laser pulse duration. A lower kinetic energy release (KER) is observed for *cis*-DCE as compared to *trans*-DCE for both fragmentation channels, which is attributed to the different conformations of the isomers. Two distinct peaks are observed in the KER spectra for both Cl^+ and HCl^+ ejection channels, indicating that two different excited states/distinct reaction pathways are involved in the dissociation process. Quantum chemical calculations reveal that the Cl^+ ejection channel follows three different pathways, one from direct C–Cl bond break-up, and the other two pathways are from intermediate states. On the other hand, HCl^+ formation is possible *via* two pathways with two intermediate states. Dissociation lifetimes of the parent ions are estimated from the angular distribution of fragments. A longer lifetime is observed for *cis*-DCE as compared to *trans*-DCE for both the fragmentation channels.

1 Introduction

The advent of ultrashort femtosecond laser pulses has enabled the study of atoms and molecules with unprecedented time resolution, which ranges from picoseconds to even attoseconds.[1–3] Further, the available peak intensity (10^{10}–10^{18} W cm^{-2}) is comparable to the potential that holds the electrons around their respective molecular nuclei, which allows the study of tunneling and related processes.[4,5] Molecules under the influence of such intense laser pulses undergo ionization (mostly single and double) through multi-photon ionization (MPI) or tunneling ionization (TI) processes based on the peak intensity. In this process, the molecules are excited from their stable neutral geometry to unstable configurations, inducing dissociation. The dissociation dynamics of molecules induced by ultrashort laser pulses has been an area of research to comprehend the nature of laser–molecule interactions, intermediate dynamical events, and the lifetime of dissociative states.[6–14] Various studies have been done to understand the role of laser pulse duration on ionization and dissociation of molecules. Sándor *et al.* reported that longer femtosecond pulses (>10 fs) influence vibrational dynamics and non-adiabatic coupling between resonant intermediate states.[15] For shorter femtosecond pulses (<10 fs), the vibrational dynamics are frozen and do not play a significant role in the ionization process.[15–17] Xie *et al.* reported that the fragmentation yield is influenced by the laser pulse duration.[18] Furthermore, how the parameters of laser pulses, such as peak intensity, wavelength, and polarization, *etc.*, can be utilized as a precise tool in regulating molecular dynamics has also been an active area of study.[6,7,9,10,19–21]

It has been shown in earlier studies that pure hydrocarbons have longer dissociation lifetimes due to the coupling between vibrational levels of excited electronic states near the dissociation state. However, the presence of halogens in the hydrocarbon molecules (*i.e.*, F, Cl, Br, I atoms replacing the hydrogen atoms) results in faster dissociation due to the availability of low-lying repulsive (n, σ*) states.[22–26]

[a] *Department of Physics, Indian Institute of Technology Dharwad, Karnataka 580011, India. E-mail: koushik.saha@iitdh.ac.in; Tel: +91-836-2309667*
[b] *Physical Research Laboratory Ahmedabad, Gujarat 380009, India. E-mail: kushawaha@prl.res.in; Tel: +91-79-26314560*
† Present address: Laboratoire d'Optique Appliquée, ENSTA ParisTech, CNRS, École Polytechnique, Palaiseau, France.
‡ Present address: European XFEL, Schenefeld, Germany.

Dichloroethylene (DCE), $C_2H_2Cl_2$, is a halogenated, colourless, volatile liquid that has two chlorine atoms on the ethylene (–CH═CH–) backbone. *Cis*- and *trans*-1,2-DCE exhibit stereo isomerization, having the same CHCl═CHCl chemical formula but differing only in the relative positions of the chlorine atoms at the two different carbons of the double bond. The double bond prevents the inter-conversion of the *cis*–*trans* isomeric states under normal conditions.[27] The dissociation of *cis*- and *trans*-1,2, DCE has attracted much attention in earlier studies.[22,28–40] Umemoto *et al.*[22] studied dissociation of *cis*- and *trans*-DCE induced by a 193 nm excimer laser. They reported the presence of two peaks in the Cl translational energy distribution and a broad translational energy distribution for the HCl fragment. They observed a lower translational energy for the Cl fragment from *cis*-DCE as compared to *trans*-DCE.

Hua *et al.*[37] carried out experiments on DCE isomers using 214.5 and 235 nm UV laser light and were able to find spin–orbit separated $Cl(^2P_J)$ in the Cl detachment. The lower peak $Cl(^2P_{3/2})$ in the energy distribution was due to the relaxation from the (π, π^*) excited state to vibrational levels of the ground state and the higher peak $Cl(^2P_{1/2})$ is ascribed to the predissociation caused by the curve crossing of the excited (π, π^*) to a repulsive (n, σ^*) or (π, σ^*) state. Similar to Umemoto *et al.*, they also noted the difference between the translational energies of fragments from *cis*- and *trans*-DCE. Ionization and dissociation of 1,2-DCE induced by femtosecond laser pulses have been studied recently with a focus on the three-body dissociation channel ($C_2H_2^+ + Cl^+ + Cl^+$), anisotropic angular distribution of ejected ions (C^{2+} and Cl^+) and dependence of laser intensity on ionization yield of parent ions ($C_2H_2Cl_2^+$).[29–32]

In the present study, we report on the strong-field ionization induced dissociation dynamics of *cis*- and *trans*-DCE upon interaction with femtosecond laser pulses with fixed peak intensity 7.33×10^{13} W cm^{-2} (Keldysh parameter, $\gamma \sim 1.07$) for different pulse durations (25 fs, 75 fs, and 180 fs). The study focuses on the two-body dissociation channels that yield Cl^+ and HCl^+ ions upon fragmentation of the doubly ionized molecular ion. The dynamics of these fragmentation channels for the ultrafast ionization regime used in this study have not been previously reported. Ion momentum spectroscopy with multi-ion coincidence detection is employed to gain complete kinematic information for the fragment ions. Fragment momentum distribution, kinetic energy release, and angular distribution are studied to bring out the dynamics of the fragmentation channels. Further, quantum chemical calculations are done to reveal the possible dissociation pathways involved in the two-body fragmentation.

2 Methods

2.1 Experimental

The experiment on the strong-field ionization of *cis*- and *trans*-DCE induced by using femtosecond laser pulses is performed in a COLTRIMS (COLd Target Recoil Ion Momentum Spectroscopy) setup. Details about the COLTRIMS setup and its capabilities have been previously reported.[7] Here, we discuss the experimental methodology. The schematic of the experiment is shown in Fig. 1. A Ti-sapphire femtosecond (coherent) laser (25 fs, 800 nm, 1 kHz, and 10 mJ) beam was utilized to ionize the molecules in the interaction region of the COLTRIMS setup. Only 3 W of power was dedicated to this experiment. A combination of a polarizer and a half-wave plate was used to adjust the power and polarization of the laser. The polarization was kept parallel to the detector plane of the spectrometer throughout the data acquisition.

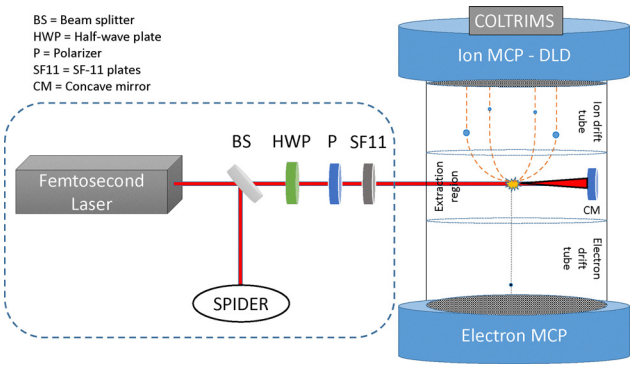

Fig. 1 Schematic diagram of experimental setup. A Ti-sapphire femtosecond (coherent) laser (25 fs, 800 nm, 1 KHz, and 3 W) beam was used in the COLTRIMS setup for the photoionization experiments. The polarization of laser pulses was parallel to the detector plane. The chamber pressure and detector parameters were kept fixed during the experiment.

Laser pulses were characterized using a commercial SPIDER (Spectral Phase Interferometry for Direct Electric field Reconstruction) setup. SF11 windows of different thicknesses were used to stretch the laser pulses to different durations. Each chirped pulse was characterized in the SPIDER setup before it entered the spectrometer. The laser pulse duration for different thicknesses of SF11, group delay dispersion (GDD), and peak power used in the experiment are summarized in Table 1.

The *cis*- and *trans*-1,2-dichloroethylene samples in the vapor phase (Sigma Aldrich, purity: >97%) are introduced into the spectrometer using an effusive needle of diameter 250 μm. At the interaction region, gas molecules interact with a laser beam focused by a concave mirror ($f = -10$ cm) in a crossed-beam fashion. The event rate was about $\lesssim$300 Hz during data acquisition. The vacuum in the chamber without a molecular sample was about 3×10^{-9} mbar, and in the presence of the molecular sample, the vacuum was about 7×10^{-8} mbar.

Time of flight and position information of fragment ions at the MCP-DLD (Micro Channel Plate and Delay Line Detector) are recorded event by event using RoentDek's TDC8HP card and related electronics. Data acquisition and analysis were performed using COBOLD PC software (RoentDek).

2.2 Computational

The quantum chemical calculations were performed in Gaussian-16 software.[41] Both *cis*- and *trans*-DCE molecular structures and their fragment derivatives before and after dissociation in neutral and ionized states were constructed.

Table 1 The characterization of laser pulses maintained throughout the experiment

SF 11 plate thickness (mm)	GDD[a] (fs^2)	Pulse duration (fs)	Energy per pulse (μJ)	Peak intensity ($W\ cm^{-2}$)
0	0	25	9	7.34×10^{13}
5	637.58	75	26.5	7.34×10^{13}
10	1607.30	180	63.5	7.33×10^{13}

[a] Group delay dispersion.

The geometry optimization and single point energy calculations were performed at the MP2/cc-pVDZ level of theory as it resembles the neutral DCE structure obtained from microscopic and electron diffraction studies.[42–45] In addition, transition state and intermediate (isomerized) state structures were calculated to check the dynamics obtained from the experimental results. All calculations were performed only in the ground state (singlet) geometry of the molecular structures.

3 Results and discussion

3.1 The mass spectrum

The *cis*- and *trans*-DCE molecules undergo extensive fragmentation upon strong-field ionization. In this work, linearly polarized femtosecond laser pulses of wavelength 800 nm at a fixed peak intensity of 7.33×10^{13} W cm^{-2} for various pulse durations were used to study the dissociative ionization. It has been reported that stretching the femtosecond laser pulses influences the ionization rate and fragmentation dynamics.[6,7] The calibrated TOF mass spectra of *cis*- and *trans*-DCE for pulse durations of 25 fs, 75 fs, and 180 fs are shown in Fig. 2. The normalization was done with respect to the total counts in each TOF spectrum. The resultant spectrum was further rescaled to 1 using the peak value of the most intense TOF peak.

The observed fragments H^+, CH_n^+, $C_2H_n^+$, Cl^+, CH_nCl^+, $C_2H_nCl^+$ (n = 0, 1, 2) indicate extensive fragmentation of ionized DCE molecules. Similar TOF mass spectra were also observed by Wada *et al.*[30] for *cis*- and *trans*-DCE. The peaks associated with Cl isotopes are also observed in the spectrum. Since the abundance of ^{37}Cl is much less and can be well distinguished from ^{35}Cl, only ^{35}Cl is considered for the reported results. As evident from Fig. 2, the fragment ion yields are affected by the change in pulse duration. Interestingly, H_2^+ ion is also observed (shown in the inset of Fig. 2), which is formed due to the bond association process. The hydrogen migration and association process also yield the HCl^+ fragment which is not resolved from Cl^+ in the TOF spectrum due to the momentum spread of these fragments. The fragmentation channels producing these fragment ions can be resolved in the photoion–photoion coincidence spectrum (see the SI, Fig. S1) which is discussed in detail in the next section.

3.2 Two-body fragmentation: Cl^+ and HCl^+ formation

The multiple fragmentation channels for the photodissociation of *cis*- and *trans*-DCE are observed in the photoion–photoion coincidence spectrum (see the SI, Fig. S1). In this work, we focus on the two-body fragmentation channels that produce Cl^+ and HCl^+ from *cis*- and *trans*-1,2-DCE dications, namely:

$$\text{(I)}\ C_2H_2Cl_2^{2+} \rightarrow Cl^+ + C_2H_2Cl^+$$

$$\text{(II)}\ C_2H_2Cl_2^{2+} \rightarrow HCl^+ + C_2HCl^+$$

The yields of the Cl^+ and HCl^+ ejection channels as a function of the pulse duration are shown in Fig. 3. The

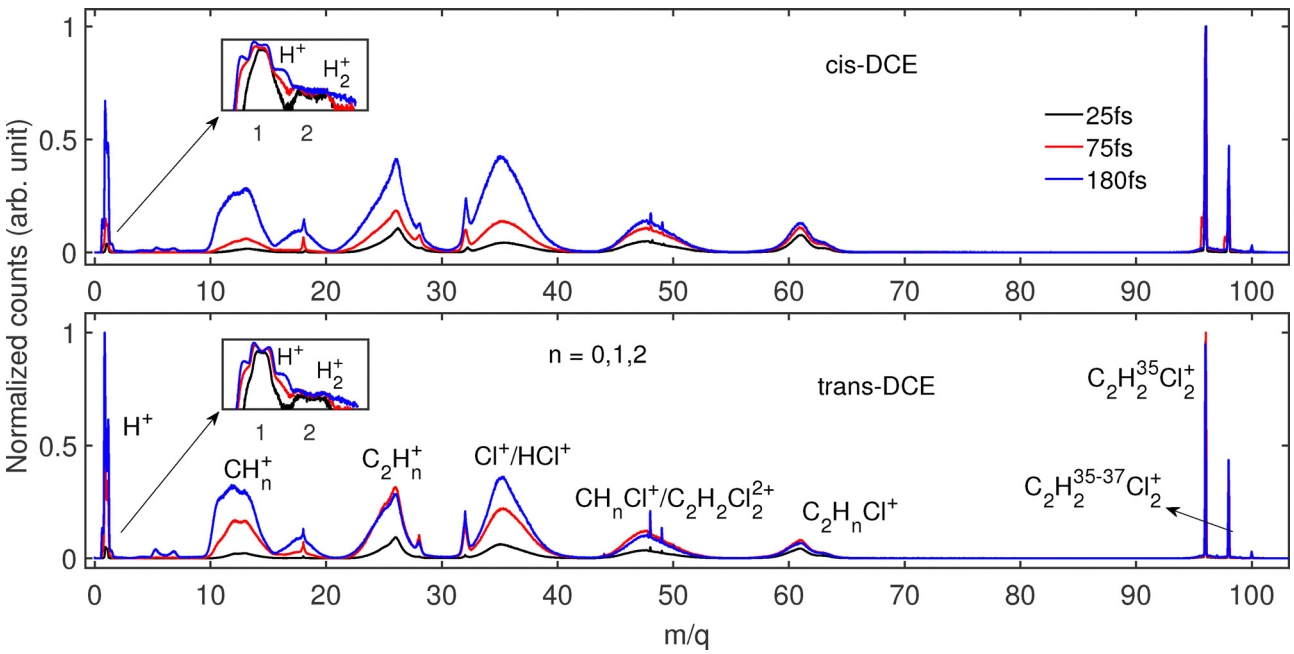

Fig. 2 Calibrated mass spectra of *cis*-DCE [top] and *trans*-DCE [bottom] recorded for linearly polarized laser pulses at 25, 75, and 180 fs pulse durations and fixed peak intensity.

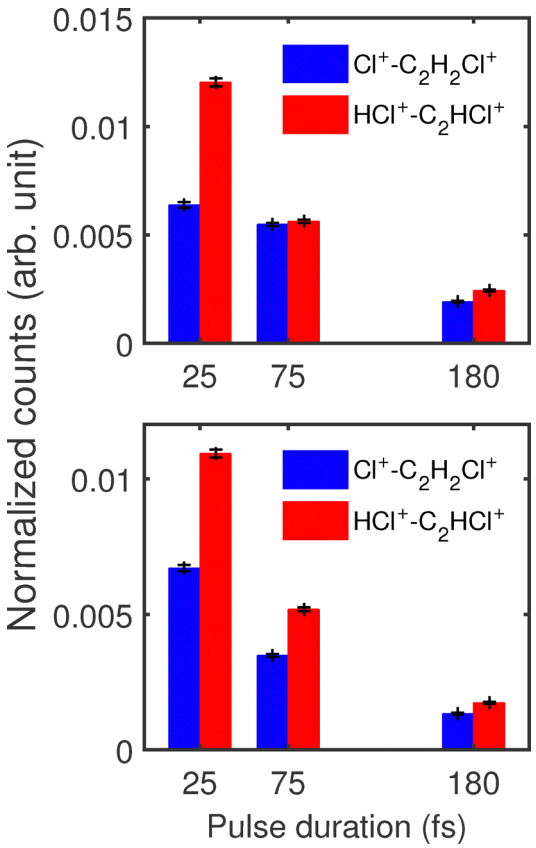

Fig. 3 [Top] Normalized yields of $Cl^+ + C_2H_2Cl^+$ and $HCl^+ + C_2HCl^+$ channels as a function of pulse durations for *cis*-DCE. [Bottom] Normalized yields of $Cl^+ + C_2H_2Cl^+$ and $HCl^+ + C_2HCl^+$ channels as a function of pulse durations for *trans*-DCE.

normalization of each dissociation channel (Cl and HCl ejection channels) was done with respect to the total counts observed in the photoion–photoion coincidence spectrum. The Cl^+ ejection channel yield for *cis*-DCE decreases by 14.03% and 69.80% at 75 fs and 180 fs compared to 25 fs. But in the case of *trans*-DCE, the Cl^+ channel decreases by 48.02% and 80.07% at 75 fs and 180 fs respectively, from the yield at 25 fs. The HCl^+ ejection channel also shows a similar trend of decreasing yield with pulse duration compared to that at 25 fs. The HCl^+ channel from *cis*-DCE decreases in yield by 53.22% and 79.69% at 75 fs and 180 fs, respectively. Similarly, in the case of *trans*-DCE, the yield of the HCl^+ ejection channel reduces at 75 fs and 180 fs by 52.49% and 84.09%. As the molecule spends more time in the intense field of the laser pulse, it gains more energy from the field. As a result, excitation to higher excited states occurs causing multi-body dissociation. We observe that the HCl^+ ejection channel has more yield than the Cl^+ ejection channel at all three pulse durations, although the yields of both decrease with pulse durations. A similar observation for acetonitrile molecule has been reported recently.[46]

The formation of HCl^+ indicates a bond rearrangement prior to dissociation of *cis*- and *trans*-DCE. In the neutral molecule, the hydrogen is bonded to the carbon atom. During dissociation, the hydrogen–carbon bond breaks, and a new bond is formed between hydrogen and chlorine. This hydrogen migration gives rise to an isomerized intermediate state $[HCl–C_2HCl]^{2+}$. The HCl^+ fragment ion is then ejected due to the rupture of the bond between HCl and carbon to yield the $HCl^+ + C_2HCl^+$ channel. The $Cl^+ + C_2H_2Cl^+$ fragmentation channel is formed due to Cl^+ ejection either from the isomerized intermediate state $[HCl–C_2HCl]^{2+}$ or by direct dissociation of the C–Cl bond. The possible fragmentation pathways for these channels are studied in detail by quantum chemical calculations discussed in the next section.

3.3 Quantum chemical calculations

The primary aim of performing quantum chemical calculations is to find out the possible dissociative reaction pathways involved in the ejection of Cl^+ and HCl^+ along with their respective counterparts from the doubly ionized DCE molecule. First, the neutral and doubly ionized molecular geometries are constructed in their equilibrium state and optimized for their respective energy and frequency. For single-point energy calculations and frequency-optimization of both isomer geometries, the MP2/cc-pVDZ functional–basis set combination is used as it converges to neutral geometry parameters close to bond parameters obtained for *cis*-DCE (bond parameters are C═C: 1.34 Å, C–H: 1.09 Å, C–Cl: 1.72 Å, ∠C–C–Cl: 124.77° and ∠C–C–H: 119.94°) and *trans*-DCE (bond parameters are C═C: 1.34 Å, C–H: 1.09 Å, C–Cl: 1.73 Å, ∠C–C–Cl: 121.21° and ∠C–C–H: 123.21°) molecules in the earlier electron diffraction and microwave spectroscopic studies.[42–45] The transition states (TS) and isomerized intermediate states (IS) involved in the formation of fragment ions Cl^+, HCl^+, $C_2H_2Cl^+$, and C_2HCl^+ are calculated, and the reaction pathways are shown in Fig. 4. It is observed that after double ionization, the bond distance of the C–Cl bond in *cis*- and *trans*-DCE reduces to 1.59 Å meanwhile the C–HCl bond distances from intermediate states IS1 and IS2 for HCl formation from *cis*-DCE are 1.64 Å and 1.76 Å respectively and from *trans*-DCE are 1.73 Å and 1.76 Å respectively. The longer bond distances always indicate weaker bonds that are likely to dissociate. The energy of the molecule is represented as the sum of electronic and zero-point energies plus zero-point correction obtained from the calculation. The energy of the ground state of the neutral molecule is taken as the reference (E_0 = 0 eV) for *cis*- and *trans*-DCE independently, and the energies (E) of all ion states are plotted relative to it, that is $\Delta E = E - E_0$ of each ion state is shown in parentheses in Fig. 4. The difference in ground state energy between neutral *cis*- and *trans*-DCE is negligible (0.00436 eV). The different ionic states of the *cis*- and *trans*-DCE are shown separately in Fig. 4 only if their energies are different up to two decimal places.

Riehl *et al.*[40] have discussed various migration and elimination channels of HCl, H_2 and Cl_2 fragments through the possible 3- and 4-center processes in DCE molecules. In our calculations as depicted in Fig. 4, the Cl^+ ejection can be possible either by a direct process by C–Cl bond breakup (marked by a black dotted line) or through any intermediate states. The HCl^+ ejection is possible only upon migration of the H atom after the H–C bond

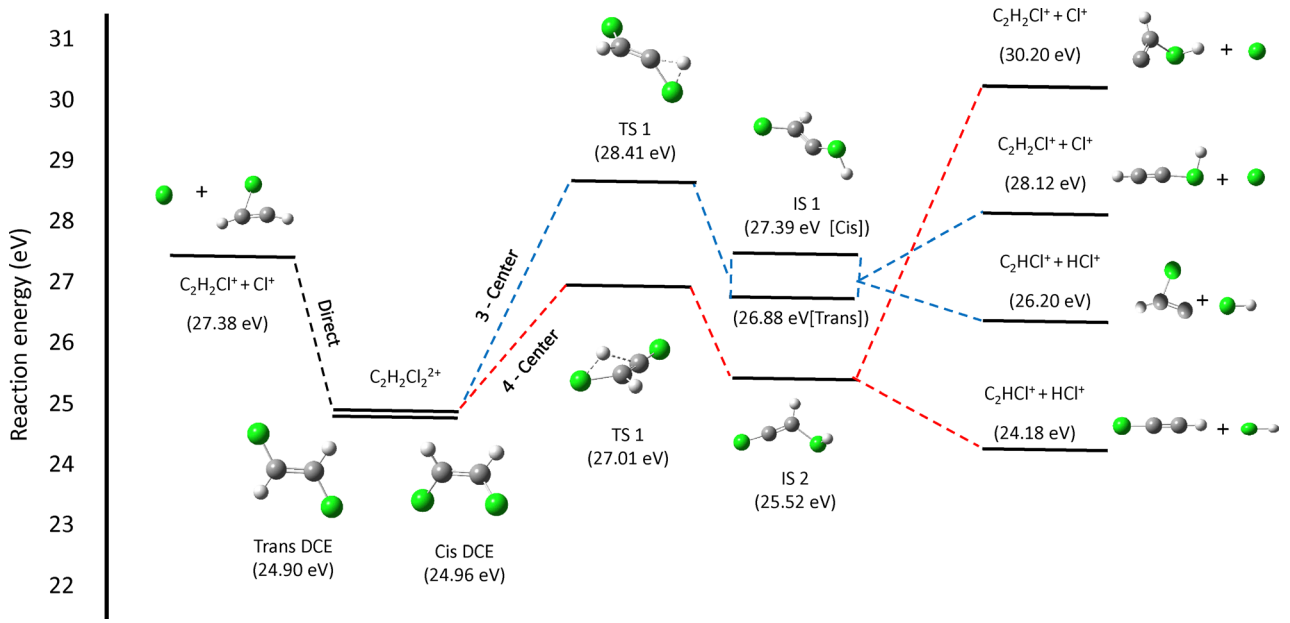

Fig. 4 Dissociation pathways for $Cl^+ + C_2H_2Cl^+$ and $HCl^+ + C_2HCl^+$ channels of *cis*- and *trans*-DCE from their doubly ionized parent molecule in the ground state. MP2/cc-pVDZ level of theory was used for the calculation of states in each dissociation pathway. All intermediate and transition states involved in the dissociation of *cis*- and *trans*-DCE have been evaluated relative to their corresponding neutral ground state (*i.e.*, with E_0 = 0 eV).

breakup and formation of the H–Cl bond followed by the breakup of C–Cl bond. The HCl formation in *cis*- and *trans*-DCE can occur mainly in two ways: 3-center HCl formation, Cl–C–H: when H migrates to the Cl atom of the same carbon atom (marked by a blue dotted line), and 4-center HCl formation, Cl–C═C–H: when the H atom from one carbon atom migrates to the Cl of the other carbon (marked by a red dotted line).

3-Center and 4-center processes of HCl^+ formation occur with the intermediate states, which are represented as IS1 (for *cis* ΔE = 27.39 eV and for *trans* ΔE = 26.88 eV) and IS2 (ΔE = 25.52 eV for both isomers) respectively. These are formed from the double ionized $C_2H_2Cl_2^{2+}$ parent ion (for *cis* ΔE = 24.96 eV and for *trans* ΔE = 24.90 eV). These intermediate states can contribute to the HCl^+ ejection as well as Cl^+ ejection depending on the excitation energy imparted by the laser pulse. It is apparent that the $HCl^+ + C_2HCl^+$ (3-centre, ΔE = 26.20 eV and 4-centre, ΔE = 24.18 eV for both isomers) formation pathway is energetically more favourable than any Cl^+ ejection dissociation pathway whether it is from direct dissociation (ΔE = 27.38 eV for both isomers) or dissociation from the intermediate states (3-centre, ΔE = 28.12 eV and 4-centre, ΔE = 30.20 eV for both isomers). This explains the results discussed in Section 3.2 where the HCl^+ ejection channel yield is greater than the Cl^+ ejection channel for all three laser pulse durations. Two distinct peaks are observed in the KER distribution (Section 3.4) for Cl^+ and HCl^+ ejection channels from both *cis*- and *trans*-DCE, indicating multiple reaction pathways involved in dissociation as apparent from the quantum chemical calculations.

3.4 KER distribution of Cl^+ and HCl^+ ejection channels

The KER distribution obtained for the $Cl^+ + C_2H_2Cl^+$ channel is shown in Fig. 5. The normalization was done with respect to the total counts for the Cl^+ dissociation channel obtained from the photoion–photoion coincidence spectrum for *cis*- and *trans*-DCE independently. The KER peak positions and range show no considerable change for different laser pulse durations, implying that the excited states involved and the dissociation mechanisms followed are independent of pulse durations. However, we observe a change in relative yield with laser pulse durations, which indicates that the probability to access particular excited states changes with pulse durations. This change is more prominent in *cis*-DCE than for *trans*-DCE. The presence of two distinct peaks *i.e.*, low and high energy components, observed in the KER distribution for both *cis*- and *trans*-DCE indicates that the dissociation *via* the $Cl^+ + C_2H_2Cl^+$ channel involves two different excited states/two distinct reaction pathways. The lower and higher KER components for *cis*-DCE are centered around 0.19 eV and 0.68 eV, respectively, while for *trans*-DCE, these are around 1.05 eV and 3.02 eV, respectively.

A similar pattern in KER distribution is observed for the $HCl^+ + C_2HCl^+$ channel shown in Fig. 6 with low and high KER components. The normalization was done with respect to the total counts of the HCl^+ dissociation channel obtained from the photoion–photoion coincidence spectrum for *cis*- and *trans*-DCE independently. For *cis*-DCE, the KER peaks are centered around 0.31 eV and 0.66 eV, respectively, while for *trans*-DCE, these are around 1.07 eV and 2.76 eV, respectively. The difference in the KER between *cis*- and *trans*-DCE is attributed to differences in their molecular geometry. According to the molecular geometry as depicted in Fig. 4, one Cl atom is bonded to each of the carbon atoms. In *cis*-DCE, two chlorine atoms are on the same side of the C═C double bond (C_{2v} symmetry) whereas, the two chlorine atoms are on two different sides of the double bond when it comes to the *trans* geometry (C_{2h} symmetry). Therefore, for *cis*-DCE, during the

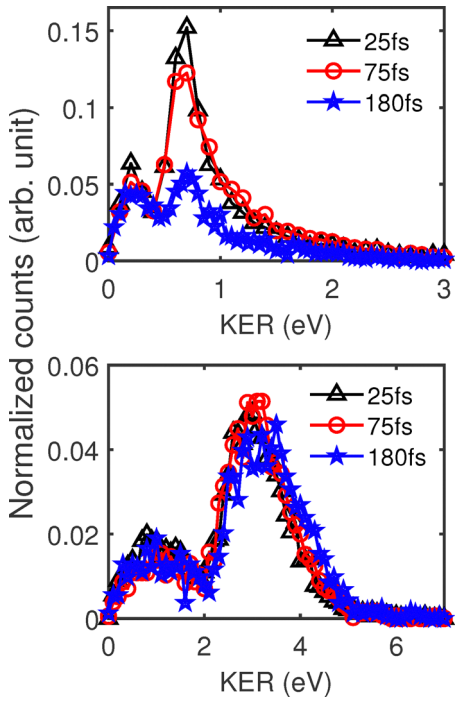

Fig. 5 KER distribution of the Cl^+ + $C_2H_2Cl^+$ channel at different pulse durations for [top] *cis*-DCE and [bottom] *trans*-DCE.

C–Cl bond breakup a high rotational force is imparted on the centre of mass (C.M.) position of the remaining part (C_2H_2Cl) since the Cl atom and the C.M. point of the remaining part of the molecule are on the same side of the double bond. On the contrary,

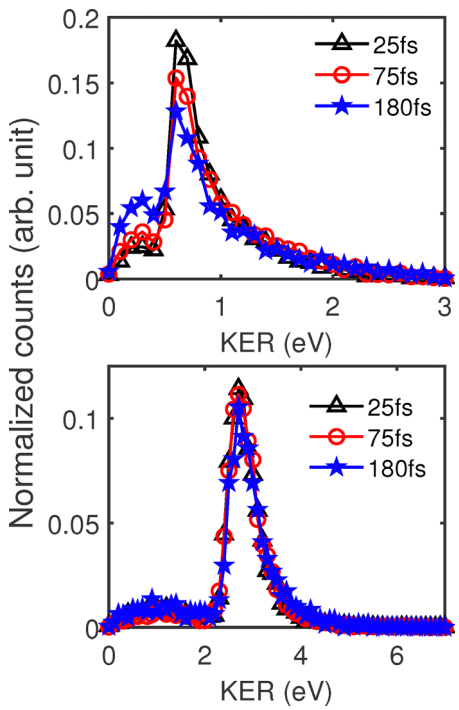

Fig. 6 KER distribution of the HCl^+ + C_2HCl^+ channel at different pulse durations for [top] *cis*-DCE and [bottom] *trans*-DCE.

the rotational force is lesser for *trans*-DCE, where ejecting the Cl atom and the C.M. point of the rest of the molecule are directed almost opposite to one another. Therefore for *cis*-DCE, the excitation energy gained by the molecule from the laser pulse is used up more towards the rotational degrees of freedom hence decreasing the energy available for translational kinetic energy of the fragments as compared to that of *trans*-DCE. This rotational shift in *cis*-DCE in comparison to *trans* is evident from rotational and vibrational studies[37,43] in DCE where the principal rotational constant of the *cis*-DCE molecule is five times lower than the *trans*-DCE molecules. The lower and higher energy components in KER might be from the direct dissociation of the molecule in the bound excited state and indirect dissociation from a steep repulsive excited state crossing with the bound excited state.[22,37,39,47,48] The difference in KER can also arise from dissociation through different intermediate geometries. From the results obtained by quantum chemical calculations, HCl^+ ejection possibly occurs from two intermediate states, IS1 and IS2. The HCl^+ ejection channel from IS2 might contribute to the high KER component as it is more energetically favorable, while the low KER component possibly comes from the IS1 state. The Cl^+ ejection can be possible in three ways: one from direct dissociation from $C_2H_2Cl_2^{2+}$ and the other two from the intermediate states with IS2 contributing to high KER and IS1 to low KER components. A double-peaked energy distribution was also reported for the translational energy of the Cl atom ejected from *cis*- and *trans*-DCE upon photodissociation by UV photons.[37] The low-energy component was attributed to dissociation from the vibrationally hot ground state after internal conversion from higher states yielding a high dissociation lifetime. In contrast, the dissociation lifetime for the low energy KER component derived from angular distribution of Cl^+ in our study is relatively low indicating a different process than observed in previous studies. The dissociation lifetimes of the fragmentation channels is discussed in the next section.

3.5 Angular distribution of Cl^+ and HCl^+ ejection channels

The angular distribution of Cl^+ and HCl^+ ion ejection with respect to the laser polarization direction is shown in Fig. 7 and 8 respectively. It is evident that the ejection from the *trans*-DCE molecule is more anisotropic than from the *cis*-DCE molecule, which suggests that the *trans* molecule dissociates faster than the *cis* molecule for both the Cl^+ and HCl^+ dissociation channels (given as [I] and [II] in Section 3.2).[22,35,37] This is due to the high rotational force acting on *cis* molecules thus increasing the dissociation time in the laser field, forming an isotropic distribution with respect to the laser polarization direction.

In earlier studies,[7,11–14,49] the anisotropy parameter was used to understand the nature of the angular distribution of the fragment and the lifetime of dissociation. The theoretical angular distribution of the fragment was obtained by fitting the experimental data on eqn (1). Anisotropy parameters were obtained from the theoretical fit to the experimental data. The angular distribution curves from experiment and theory are given in Fig. 7 and 8 respectively.

$$I(\theta) \propto 1 + \sum_L a_L P_L \cos(\theta) \quad (\text{where} \quad L = 2, 4, 6) \qquad (1)$$

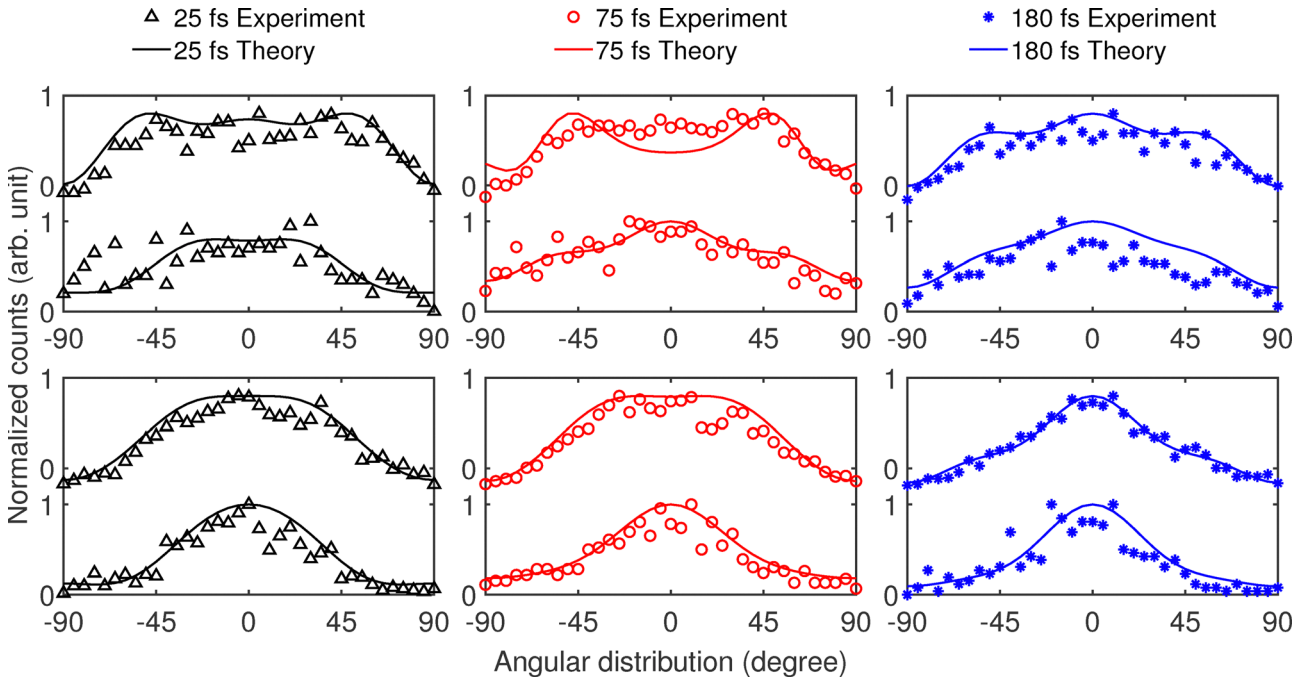

Fig. 7 Angular distribution of Cl^+ with respect to laser polarization axis for *cis*- (1st row) and *trans*-DCE (2nd row) for the $Cl^+ + C_2H_2Cl^+$ fragmentation channel. In each plot, the top curve shows the angular distribution for the high-energy component of KER and the bottom curve shows the angular distribution for the low-energy component of KER.

The expansion coefficients a_L are the anisotropy parameters and $P_L\cos(\theta)$ are the Legendre polynomials of orders $L = 2, 4, 6$, respectively. $I(\theta)$ represents the angular distribution and θ is the angle between the direction of the laser polarization and the recoil velocity of the ejected fragment. A positive anisotropy parameter, especially $a_2 > 1$, indicates more anisotropy in the angular distribution of fragments. The estimated anisotropic parameters presented in Table 2 show that fragmentation from

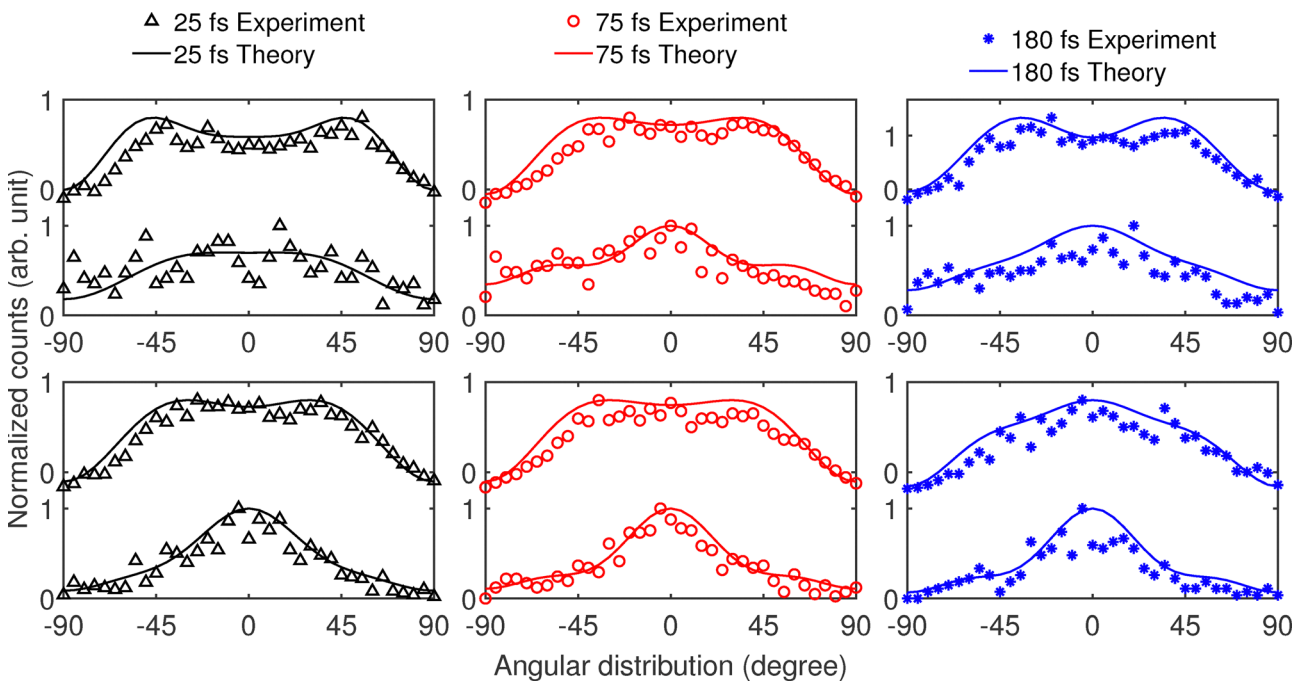

Fig. 8 Angular distribution of HCl^+ with respect to laser polarization axis for *cis*- (1st row) and *trans*-DCE (2nd row) for the $HCl^+ + C_2HCl^+$ fragmentation channel. In each plot, the top curve shows the angular distribution for the high-energy component of KER and the bottom curve shows the angular distribution for the low-energy component of KER.

Table 2 The anisotropy parameters for the Cl^+ + $C_2H_2Cl^+$ and HCl^+ + C_2HCl^+ dissociation channels

Fragment ion	a_2		
cis-DCE	25 fs	75 fs	180 fs
Cl^+	0.75	0.82	0.82
HCl^+	0.74	0.99	1.00
trans-DCE	25 fs	75 fs	180 fs
Cl^+	1.62	1.48	1.70
HCl^+	1.26	1.21	1.38

trans-DCE is more anisotropic than that from *cis*-DCE. These findings also suggest that fragments ejected from precursors with higher rotational motion have less anisotropy in angular distribution, as reported in previous studies.[7,11–14]

3.6 Dissociation lifetime (τ) of Cl^+ and HCl^+ ejection channels

The dissociation lifetime (τ) of the fragmentation channels can be obtained by fitting the angular distribution with the molecular rotational parameter $C_L(\tau\omega)$ as given in eqn (2):[11–14]

$$I(\theta, \tau\omega) = 1 + \sum_L C_L a_L P_L \cos(\theta) \quad (\text{where} \quad L = 2, 4, 6) \quad (2)$$

Rotational parameter $C_L(\tau\omega)$ is a function of dissociation lifetime τ and angular frequency of rotation (ω) and $\tau\omega$ can be determined from C_L using eqn (3):

$$C_L = \prod_k^{\frac{L}{2}} \frac{(1/\tau\omega)^2 + (2k-1)^2}{(1/\tau\omega)^2 + (2k)^2} \quad (\text{where} \quad L = 2, 4, 6) \quad (3)$$

The angular frequency of rotation (ω) is calculated from the rotational time period of the molecule (τ_{rot}) as given in eqn (4):

$$\tau_{rot} = \frac{2\pi}{\sqrt{\pi KT(B_0/\hbar^2)}}; \quad \text{and} \quad \omega = \frac{2\pi}{\tau_{rot}} \quad (4)$$

The rotational constants (B_0) for *cis*- and *trans*-DCE were obtained from infrared spectroscopic studies done earlier[43,50] as 0.38421 cm^{-1} and 1.74726 cm^{-1} respectively at temperature T = 300 K. τ_{rot} and ω determined for *cis*- and *trans*-DCE are given below:

$$\tau_{rot} = 3.00 \text{ ps}; \quad \omega = 2.09 \text{ ps}^{-1} \quad \text{for } cis\text{-DCE}$$

$$\tau_{rot} = 0.98 \text{ ps}; \quad \omega = 6.40 \text{ ps}^{-1} \quad \text{for } trans\text{-DCE}$$

The difference in rotational period of *cis*- and *trans*-DCE molecules causes the observed difference in KER, as mentioned in Section 3.4.

The dissociation lifetime (τ) is obtained after using the value of ω in the expression $\tau\omega$ calculated from C_L parameters for the *cis*- and *trans*-DCE. Tables 3 and 4 show the dissociation lifetime (τ) of *cis*- and *trans*-DCE channels for the low and high energy components of the KER distribution. As discussed in Section 3.4, in the KER distribution of *cis*- and *trans*-DCE, the presence of two distinct peaks gives information about two different reaction pathways through which molecular dissociation is possible. Overall, we observe that the dissociation lifetime of *trans*-DCE is lower than that of *cis*-DCE. This can be attributed to the higher rotational motion of the precursor molecular ion of *cis*-DCE as compared to *trans*-DCE. The dissociation lifetimes for the Cl^+ and HCl^+ ejection channels are the same, indicating the possibility of a similar dissociation mechanism in both cases instead of concerted breakup. It is observed that the dissociation lifetimes for lower and higher KER components of the Cl^+ and HCl^+ ejection channels are similar for both *cis*-DCE (~400 fs) and *trans*-DCE (~180 fs). Further, no change in lifetime is observed as a function of the laser pulse duration. The calculated lifetime for the Cl^+ ejection channel for the high KER component is similar to that obtained by pump–probe studies performed on DCE.[35,37] However, the dissociation lifetime for the low KER component is different from those obtained for DCE by Farmanara *et al.*[35] and Hua *et al.*,[37] indicating a different dissociation mechanism in our study.

Table 3 The dissociation lifetime (τ) of the Cl^+ + $C_2H_2Cl^+$ and HCl^+ + C_2HCl^+ dissociation channels from *cis*-DCE for low and high energy components of the KER distribution

	τ (fs)					
	25 fs		75 fs		180 fs	
cis-DCE channels	Low KER	High KER	Low KER	High KER	Low KER	High KER
$Cl^+ + C_2H_2Cl^+$	398.79	434.21	424.56	424.21	407.52	427.83
$HCl^+ + C_2HCl^+$	397.10	435.43	439.63	412.58	410.54	420.74

Table 4 The dissociation lifetime (τ) of the Cl^+ + $C_2H_2Cl^+$ and HCl^+ + C_2HCl^+ dissociation channels from *trans*-DCE for low and high energy components of the KER distribution

	τ (fs)					
	25 fs		75 fs		180 fs	
trans-DCE channels	Low KER	High KER	Low KER	High KER	Low KER	High KER
$Cl^+ + C_2H_2Cl^+$	181.60	175.90	185.31	176.28	187.62	187.46
$HCl^+ + C_2HCl^+$	186.09	181.00	191.99	181.37	192.15	180.26

4 Conclusion

A comparative study of the dissociation dynamics of *cis*- and *trans*-1,2-DCE has been done employing femtosecond laser pulses of varying pulse duration (25, 75, and 180 fs) with particular focus on Cl^+ + $C_2H_2Cl^+$ and HCl^+ + C_2HCl^+ dissociation channels. An increase in the ion yield of the fragment ions and a decrease in the yield of the singly charged parent ion ($C_2H_2Cl_2^+$) in the TOF spectrum have been observed with increase in laser pulse duration. A pattern of diminishing yields for Cl^+ + $C_2H_2Cl^+$ and HCl^+ + C_2HCl^+ dissociation channels upon increase in laser pulse duration is observed. Both the changes in ion yield and dissociation channel yield indicate enhanced ionization and fragmentation as a function of laser pulse duration. The HCl^+ ejection channel yield was observed to

be higher than that of the Cl^+ ejection channel for both the isomers.

For both $Cl^+ + C_2H_2Cl^+$ and $HCl^+ + C_2HCl^+$ dissociation channels, a higher KER is observed for *trans*-DCE as compared to *cis*-DCE. The excitation energy spent for the rotational motion is more for *cis*-DCE molecules than that of the *trans* molecules due to the geometry of the isomers. Thus, less energy is reflected in the KER for *cis*-DCE as compared to that of *trans*-DCE. The existence of two distinct peaks in the KER distribution signifies the availability of two reaction pathways through which dissociation is possible for both the channels as indicated by theoretical calculations. There was no significant change in the KER with respect to the laser pulse duration.

The anisotropic parameters (a_L) were obtained from the angular distribution of the Cl^+ and HCl^+ fragments. These parameters have higher positive values for *trans*-DCE compared to those of *cis*-DCE, which evince that the *trans* channels are more anisotropic than those of *cis* as a result of the lower rotation of the precursor molecule before the dissociation. Dissociation lifetimes of the $Cl^+ + C_2H_2Cl^+$ and $HCl^+ + C_2HCl^+$ channels were calculated from the rotational parameters (C_L) and rotational frequencies (ω) for *cis*- and *trans*-DCE separately. The calculated lifetimes of the *cis* and *trans* isomers are very different, irrespective of the dissociation channel (*cis*-DCE $\sim$ 400 fs and *trans*-DCE $\sim$ 180 fs). There is no change in the lifetimes with respect to the laser pulse duration. Both KER distribution and dissociation lifetime of the Cl^+ and HCl^+ ejection channels are very similar. This may be due to the close resemblance of the geometries of the precursors since the displacement of the light-mass hydrogen atom from carbon (H–C) to chlorine (H–Cl) is the only difference when it comes to the HCl^+ and Cl^+ ejection. This suggests an ultrafast H-migration and association producing HCl^+.

Author contributions

RKK, RD and KS planned the research. RD, VN, MP, PB, PC, EA, KS and RKK worked on the experiments. EA, RD, RKK and KS performed the data analysis. The quantum chemical calculations were performed by EA and KS. The first draft was prepared by EA, RKK and KS, and other team members contributed to the final manuscript.

Conflicts of interest

There are no conflicts to declare.

Data availability

The paper presents the strong field ionization and dissociation of *cis*- and *trans*-DCE based on experimental measurements of time of flight (TOF), kinetic energy release (KER) and angular distribution of fragments; therefore, the measured data are reported and are available in the paper itself (see Fig. 2, 3 and 5–8) and in the supplementary information (SI). Supplementary information is available. See DOI: https://doi.org/10.1039/d5cp03038b.

Acknowledgements

KS, RKK and EA acknowledge DST-ANRF, India for providing financial support under the Core Research Grant (CRG/2022/006578). RKK, VN and PC acknowledge PRL, DOS and GOI support for the research activities of the Femtosecond Laser Lab, PRL, Ahmedabad.

References

1 J. M. Dahlström, A. L'Huillier and A. Maquet, *J. Phys. B: At., Mol. Opt. Phys.*, 2012, **45**, 183001.
2 A. Maquet, J. Caillat and R. Taïeb, *J. Phys. B: At., Mol. Opt. Phys.*, 2014, **47**, 204004.
3 M. Huppert, I. Jordan, D. Baykusheva, A. Von Conta and H. J. Wörner, *Phys. Rev. Lett.*, 2016, **117**, 093001.
4 S. Popruzhenko, *J. Phys. B: At., Mol. Opt. Phys.*, 2014, **47**, 204001.
5 P. B. Corkum, *Phys. Rev. Lett.*, 1993, **71**, 1994.
6 R. Das, D. K. Pandey, V. Nimma, M. P., P. Bhardwaj, P. Chandravanshi, M. Shameem K. M., D. K. Singh and R. K. Kushawaha, *Faraday Discuss.*, 2021, **228**, 432–450.
7 R. Das, D. K. Pandey, S. Soumyashree, P. Madhusudhan, V. Nimma, P. Bhardwaj, M. S. K. M., D. K. Singh and R. K. Kushawaha, *Phys. Chem. Chem. Phys.*, 2022, **24**, 18306–18320.
8 R. Das, A. K. Bhojani, V. Nimma, P. Bhardwaj, D. K. Singh and R. K. Kushawaha, *et al.*, *J. Phys. B: At., Mol. Opt. Phys.*, 2025, **58**, 045603.
9 S. Bhattacharyya, K. Borne, F. Ziaee, S. Pathak, E. Wang, A. S. Venkatachalam, N. Marshall, K. D. Carnes, C. W. Fehrenbach and T. Severt, *et al.*, *Phys. Chem. Chem. Phys.*, 2022, **24**, 27631–27644.
10 S. Bhattacharyya, K. Borne, F. Ziaee, S. Pathak, E. Wang, A. S. Venkatachalam, X. Li, N. Marshall, K. D. Carnes and C. W. Fehrenbach, *et al.*, *J. Phys. Chem. Lett.*, 2022, **13**, 5845–5853.
11 S. Sun, Y. Yang, J. Zhang, H. Wu, Y. Chen, S. Zhang, T. Jia, Z. Wang and Z. Sun, *Chem. Phys. Lett.*, 2013, **581**, 16–20.
12 T. Okino, Y. Furukawa, P. Liu, T. Ichikawa, R. Itakura, K. Hoshina, K. Yamanouchi and H. Nakano, *Chem. Phys. Lett.*, 2006, **419**, 223–227.
13 A. Hishikawa, H. Hasegawa and K. Yamanouchi, *J. Electron Spectrosc. Relat. Phenom.*, 2004, **141**, 195–200.
14 B. Liu, Y. Yang, H. Sun and Z. Sun, *Molecules*, 2018, **23**, 3096.
15 P. Sándor, V. Tagliamonti, A. Zhao, T. Rozgonyi, M. Ruckenbauer, P. Marquetand and T. Weinacht, *Phys. Rev. Lett.*, 2016, **116**, 063002.
16 A. Howard, C. Cheng, R. Forbes, G. McCracken, W. Mills, V. Makhija, M. Spanner, T. Weinacht and P. Bucksbaum, *Phys. Rev. A*, 2021, **103**, 043120.
17 C. Cheng, Z. L. Streeter, A. J. Howard, M. Spanner, R. R. Lucchese, C. W. McCurdy, T. Weinacht,

P. H. Bucksbaum and R. Forbes, *Phys. Rev. A*, 2021, **104**, 023108.
18 X. Xie, E. Lötstedt, S. Roither, M. Schöffler, D. Kartashov, K. Midorikawa, A. Baltuška, K. Yamanouchi and M. Kitzler, *Sci. Rep.*, 2015, **5**, 12877.
19 K. Hoshina, T. Shirota and M. Tsuge, *J. Phys. Chem. A*, 2021, **125**, 9508–9517.
20 G. L. Gutsev, S. L. McPherson, H. A. López Pena, D. A. Boateng, L. G. Gutsev, B. R. Ramachandran and K. M. Tibbetts, *J. Phys. Chem. A*, 2020, **124**, 7427–7438.
21 U. Ablikim, C. Bomme, H. Xiong, E. Savelyev, R. Obaid, B. Kaderiya, S. Augustin, K. Schnorr, I. Dumitriu and T. Osipov, *et al.*, *Sci. Rep.*, 2016, **6**, 38202.
22 M. Umemoto, K. Seki, H. Shinohara, U. Nagashima, N. Nishi, M. Kinoshita and R. Shimada, *J. Chem. Phys.*, 1985, **83**, 1657–1666.
23 S. Larimian, S. Erattupuzha, E. Lötstedt, T. Szidarovszky, R. Maurer, S. Roither, M. Schöffler, D. Kartashov, A. Baltuška and K. Yamanouchi, *et al.*, *Phys. Rev. A*, 2016, **93**, 053405.
24 R. Bersohn, *IEEE J. Quantum Electron.*, 1980, **16**, 1208–1218.
25 M. Kawasaki, K. Kasatani, H. Sato, H. Shinohara and N. Nishi, *Chem. Phys.*, 1984, **88**, 135–142.
26 G. Ondrey and R. Bersohn, *J. Chem. Phys.*, 1983, **79**, 175–178.
27 G. M. Wyman, *Chem. Rev.*, 1955, **55**, 625–657.
28 U. Ablikim, C. Bomme, T. Osipov, H. Xiong, R. Obaid, R. C. Bilodeau, N. G. Kling, I. Dumitriu, S. Augustin and S. Pathak, *et al.*, *Rev. Sci. Instrum.*, 2019, **90**, 055103.
29 T. Yatsuhashi, N. Nakashima and J. Azuma, *J. Phys. Chem. A*, 2013, **117**, 1393–1399.
30 Y. Wada, H. Akagi, T. Kumada, R. Itakura and T. Wakabayashi, *Photochem*, 2022, **2**, 798–809.
31 S. W. Crane, J. W. Lee, M. N. Ashfold and D. Rolles, *Phys. Chem. Chem. Phys.*, 2023, **25**, 16672–16698.
32 S. Zigo, A.-T. Le, P. Timilsina and C. A. Trallero-Herrero, *Sci. Rep.*, 2017, **7**, 42149.
33 A. Bodi, W. R. Stevens and T. Baer, *J. Phys. Chem. A*, 2011, **115**, 726–734.
34 W. Zhou, L. Ge, G. A. Cooper, S. W. Crane, M. H. Evans, M. N. Ashfold and C. Vallance, *J. Chem. Phys.*, 2020, **153**, 184201.
35 P. Farmanara, O. Steinkellner, M. Wick, M. Wittmann, G. Korn, V. Stert and W. Radloff, *J. Chem. Phys.*, 1999, **111**, 6264–6270.
36 I. Hartl and W. Zinth, *J. Phys. Chem. A*, 2000, **104**, 4218–4222.
37 L. Hua, X. Zhang, W.-B. Lee, M.-H. Chao, B. Zhang and K.-C. Lin, *J. Phys. Chem. A*, 2010, **114**, 37–44.
38 M. Parkes, S. Ali, C. Howle, R. Tuckett and A. Malins, *Mol. Phys.*, 2007, **105**, 907–916.
39 T. Suzuki, K. Tonokura, L. S. Bontuyan and N. Hashimoto, *J. Phys. Chem.*, 1994, **98**, 13447–13451.
40 J.-F. Riehl, D. G. Musaev and K. Morokuma, *J. Chem. Phys.*, 1994, **101**, 5942–5956.
41 M. J. Frisch, G. W. Trucks, H. B. Schlegel, G. E. Scuseria, M. A. Robb, J. R. Cheeseman, G. Scalmani, V. Barone, G. A. Petersson, H. Nakatsuji, X. Li, M. Caricato, A. V. Marenich, J. Bloino, B. G. Janesko, R. Gomperts, B. Mennucci, H. P. Hratchian, J. V. Ortiz, A. F. Izmaylov, J. L. Sonnenberg, D. Williams-Young, F. Ding, F. Lipparini, F. Egidi, J. Goings, B. Peng, A. Petrone, T. Henderson, D. Ranasinghe, V. G. Zakrzewski, J. Gao, N. Rega, G. Zheng, W. Liang, M. Hada, M. Ehara, K. Toyota, R. Fukuda, J. Hasegawa, M. Ishida, T. Nakajima, Y. Honda, O. Kitao, H. Nakai, T. Vreven, K. Throssell, J. A. Montgomery, Jr., J. E. Peralta, F. Ogliaro, M. J. Bearpark, J. J. Heyd, E. N. Brothers, K. N. Kudin, V. N. Staroverov, T. A. Keith, R. Kobayashi, J. Normand, K. Raghavachari, A. P. Rendell, J. C. Burant, S. S. Iyengar, J. Tomasi, M. Cossi, J. M. Millam, M. Klene, C. Adamo, R. Cammi, J. W. Ochterski, R. L. Martin, K. Morokuma, O. Farkas, J. B. Foresman and D. J. Fox, *Gaussian 16 Revision C.01*, Gaussian Inc., Wallingford CT, 2016.
42 L. Schäfer, J. D. Ewbank, K. Siam, D. W. Paul and D. L. Monts, *J. Mol. Struct.*, 1986, **145**, 135–142.
43 N. C. Craig, R. A. Appleman, H. E. Barnes, E. Morales, J. A. Smith, S. Klee, M. Lock and G. C. Mellau, *J. Phys. Chem. A*, 1998, **102**, 6745–6752.
44 H. Takeo, M. Sugie and C. Matsumura, *J. Mol. Struct.*, 1988, **190**, 205–214.
45 J. B. P. D. Silva and M. N. Ramos, *J. Braz. Chem. Soc.*, 2004, **15**, 43–49.
46 Q. Ma, J. Zhou, X. Xue, X. Hao, E. Wang and X. Ren, *Phys. Rev. A*, 2025, **111**, 042817.
47 B. Gaire, J. McKenna, A. Sayler, N. G. Johnson, E. Parke, K. Carnes, B. Esry and I. Ben-Itzhak, *Phys. Rev. A: At., Mol., Opt. Phys.*, 2008, **78**, 033430.
48 S. Arulmozhiraja, M. Ehara and H. Nakatsuji, *J. Chem. Phys.*, 2008, **129**, 174506.
49 J. Cooper and R. N. Zare, *J. Chem. Phys.*, 1968, **48**, 942–943.
50 G. Herzberg, *Electronic spectra and electronic structure of polyatomic molecules*, Van Nostrand Reinhold, 1966.